







 Cite this: *RSC Adv.*, 2022, 12, 3372

# Oxidation-degree-dependent moisture-induced actuation of a graphene oxide film†

 Waka Nakanishi, <sup>\*,a</sup> Yoshihiro Yamauchi, <sup>a</sup> Yuta Nishina, <sup>b</sup>  
 Masafumi Yoshio <sup>cd</sup> and Masayuki Takeuchi <sup>ae</sup>

Multilayered films prepared from graphene oxide (GO) subjected to a single oxidation process (1GO) can actuate in response to moisture, whereas those prepared from GO subjected to two oxidation processes (2GO) lose this ability. To elucidate the origin of this difference, the structures and properties of various multilayered films and their contents were analyzed. According to atomic force microscopy images, the lateral size of the GO monolayer in 2GO ( $2.0 \pm 0.4 \mu\text{m}$ ) was smaller than that in 1GO ( $3.2 \pm 0.4 \mu\text{m}$ ), although this size difference did not affect actuation. Scanning electron microscopy images of the cross sections of both films showed fine multilayered structures and X-ray diffraction measurements showed the moisture sensitive reversible change in the interlayer distances for both films. Both films adsorbed 30 wt% moisture in 60 s with different water contents at the bottom moist sides and top air sides of the films. Nanoindentation experiments showed hardness values (1GO:  $156 \pm 67 \text{ MPa}$ ; 2GO:  $189 \pm 97 \text{ MPa}$ ) and elastic modulus values (1GO:  $4.7 \pm 1.7 \text{ GPa}$ ; 2GO:  $5.8 \pm 3.2 \text{ GPa}$ ) typical of GO, with no substantial difference between the films. On the contrary, the 1GO film bent when subjected to a weight equal to its own weight, whereas the 2GO film did not. Such differences in the macroscopic hardness of GO films can affect their moisture-induced actuation ability.

 Received 21st October 2021  
 Accepted 14th January 2022

DOI: 10.1039/d1ra07773b

[rsc.li/rsc-advances](https://rsc.li/rsc-advances)

## Introduction

Actuator materials mechanically move in response to external stimuli, such as light,<sup>1–4</sup> heat,<sup>5–7</sup> chemicals,<sup>8,9</sup> and electric<sup>10–12</sup>/magnetic<sup>13</sup> fields. For actuation, chemical structures that are changed by external energy sources and anisotropic alignment of the structures that accumulate strain to generate motion are important. Among the materials available for actuators, water-responsive materials have attracted attention because water is a ubiquitous resource.<sup>14</sup>

Polymers have been extensively studied as water-responsive actuator materials<sup>15–18</sup> because they enable the design of hydrophilic chemical structures that capture water molecules and the fabrication of anisotropic structures that trigger movement. Anisotropic structures in materials are often

fabricated by incorporating one-dimensional (1D) or two-dimensional (2D) nanoobjects, because they can be aligned in response to external stimuli such as shear force, electric force, magnetic force, compression, or stretching. Among the family of materials for 1D or 2D nanoobjects,<sup>19</sup> graphene oxide (GO) is an ideal material for moisture-responsive actuation because it features tunable hydrophilic functionalities on highly anisotropic 2D structures through the oxidation of graphite. In fact, several notable properties of GO, including high sensitivity to humidity,<sup>20–22</sup> strong power generation,<sup>23–25</sup> and short response times,<sup>26–29</sup> have been reported. In addition to these potential promising properties as an actuator, GO is a light-weight, inexpensive, bio-compatible material,<sup>19</sup> and has merits for further applications. On the other hand, because all of the hydrophilic monolayers prepared *via* the oxidation of graphite<sup>30</sup> are defined as GO, the degree of oxidation and associated properties, such as the size of the monolayers, type of hydrophilic functionality (*e.g.*, epoxy, hydroxy, carbonyl, or carboxylic acid functionalities), functional-group content, and mechanical properties of the GO, vary depending on the GO preparation procedure.<sup>31–33</sup> Thus, the relationships between the structure and moisture-responsiveness of GO have only begun to be elucidated.<sup>34</sup>

In the present work, we report on distinct differences in moisture-induced actuation of two GO thin films with different oxidation degrees. The oxidation degree of GO was tuned by varying the number of oxidation reaction cycles. GO thin films

<sup>a</sup>Molecular Design and Function Group, National Institute for Materials Science, 1-2-1 Sengen, Tsukuba, Ibaraki 305-0047, Japan. E-mail: NAKANISHI.Waka@nims.go.jp

<sup>b</sup>Research Core for Interdisciplinary Sciences, Okayama University, 3-1-1 Tsushima-naka, Okayama 700-8530, Japan

<sup>c</sup>Research Center for Functional Materials, National Institute for Materials Science, 1-2-1 Sengen, Tsukuba, Ibaraki 305-0047, Japan

<sup>d</sup>Graduate School of Chemical Sciences and Engineering, Hokkaido University, Kita 13, Nishi 8, Kita-ku, Sapporo, Hokkaido 060-8628, Japan

<sup>e</sup>Institute of Multidisciplinary Research for Advanced Materials (IMRAM), Tohoku University, Sendai 980-8579, Japan

† Electronic supplementary information (ESI) available. See DOI: 10.1039/d1ra07773b



were fabricated from GO with one-cycle oxidation (1GO) and two-cycle oxidation (2GO). Only the 1GO thin films were actuated upon moisture stimulation; no motion was observed for the 2GO films subjected to the same stimulation. Although both of the thin films exhibit the characteristic properties required for moisture actuation (*i.e.*, multilayered structures and the ability to adsorb and release moisture), we observed notable differences in their macroscopic mechanical properties. Only the 1GO film bent when loaded with a weight similar to its own weight. In this work, we show that the oxidation degree and related mechanical properties affect the moisture-actuation ability of GO films. These characteristics have been overlooked, but should be considered in the further development of GO-based materials.

## Experimental

### Materials

1GO was prepared as an aqueous suspension with a GO content of 1 wt% *via* the oxidation of graphite according to the reported method using a graphite:KMnO<sub>4</sub> ratio of 1 : 3 (w/w).<sup>35</sup> Graphite (SP-1, Bay Carbon Inc.; 3.0 g) was added to H<sub>2</sub>SO<sub>4</sub> (75 mL), and then KMnO<sub>4</sub> (9.0 g) was slowly added at 10 °C with stirring at 200 rpm. The mixture was kept at 35 °C for 2 h before quenching with H<sub>2</sub>O (75 mL) under vigorous stirring and cooling so that the temperature does not exceed 50 °C. H<sub>2</sub>O<sub>2</sub> (30%, 7.5 mL) was slowly added, with continuous stirring, for 30 min at ambient temperature. The reaction mixture was purified by centrifugation. 2GO was prepared by a similar method except that these oxidation procedures were repeated. 1GO and 2GO were obtained as dry samples by freeze-drying of the corresponding aqueous suspensions.

### Preparation of GO thin films

To a viscous aqueous suspension (2.5 g) with a 1 wt% content of 1GO, distilled water (2.5 mL) was added and the resultant mixture was stirred. A 1GO film was prepared by pouring the mixture into a polytetrafluoroethylene (PTFE) Petri dish (diameter: 50 mm) and the GO film was peeled off after it had been air-dried for more than 3 days. 1GO and 2GO films were prepared from dry 1GO or 2GO samples (25 mg) using the same method, except that aqueous suspensions of freeze-dried samples of 1GO or 2GO (25 mg each) in distilled water (5 mL) were used. A 1GO film was also prepared by vacuum filtration using a mixed cellulose ester (MCE) membrane (diameter: 47 mm, pore size: 0.45 μm), and the film was exfoliated after air-drying of the filtrate. For the preparation of a film with a fragmented 1GO sample, an aqueous suspension of 1GO was sonicated (BRANSONIC 3510J-MT) for 1 h and the resultant suspension was used to prepare a fragmented 1GO film. The thickness of the GO films was controlled from 9 to 22 μm by varying the amount of GO in the aqueous suspension.

### Characterization

The thickness of the GO films was determined using micrometer calipers (NIIGATASEIKI MCD 130-25). The size of the GO

fragments was determined by atomic force microscopy (AFM; BRUKER NanoScopeV). For AFM observations, aqueous GO suspensions were sonicated for 10 s and the resultant suspensions were spin-coated onto freshly cleaved mica substrates. AFM images were obtained in tapping mode on a Multimode 8 model scanning probe microscope. X-ray photoelectron spectroscopy (XPS; ULVAC-PHI Quantera SXM scanning X-ray microprobe, Al K $\alpha$  excitation source,  $h\nu = 1486.6$  eV) measurements were performed to characterize the surface of the 1GO and 2GO films. Ultraviolet-visible absorption spectroscopy (UV-Vis; JASCO V-670) was performed on aqueous suspensions of the GO samples. A cross section of each GO film was generated by grabbing both ends with tweezers and dividing it, and it was subsequently observed by scanning electron microscopy (SEM; JEOL, JSM-6500F). The interlayer spacing of the GO films was determined from the X-ray diffraction pattern (XRD; Rigaku Miniflex 600, Ni-filtered Cu K $\alpha$  radiation) without or with a moist substrate placed 1 cm from the GO film. The adsorption of moisture was analyzed on the basis of the weight change of the 1GO (25 mg) and 2GO (22 mg) films upon exposure to a moist substrate under conditions similar to those used in the moisture-assisted actuation tests mentioned below, without using the weight or the plastic films. Water on the film surface was analyzed using attenuated total reflection Fourier transform infrared spectra (ATR-FTIR, Thermo Scientific Nicolet NEXUS 670). A nanoindentation device (KLA, iMicro) equipped with a Berkovich indenter was used to measure the nano-mechanical properties of the films. A continuous stiffness measurement (CSM)<sup>36</sup> was carried out by superimposing small-amplitude, 110 Hz oscillations on the force signal to record stiffness data along with load and displacement data dynamically. The hardness and Young's modulus of the GO thin films were determined from the load–displacement curves corresponding to an indentation depth of 1.9–2.1 μm by the method developed by Oliver *et al.*<sup>37</sup> The distortion ( $\epsilon$ ) of the weight-loaded (20, 50 mg) 1GO and 2GO films was determined using the equation:<sup>38</sup>

$$\epsilon = 2d\delta/(L^2 + d^2),$$

where  $d$  is the thickness of the film (mm),  $\delta$  is the displacement of the film in the vertical direction (mm), and  $L$  is the distance from the fulcrum (mm) (Table S1†).

### Moisture-assisted actuation test

Moist paper (diameter: 185 mm) heated at 50 °C on a hotplate (CORNING PC-420D) was covered with dry paper (diameter: 185 mm) to avoid direct contact of water with the GO films. Plastic films were placed between these papers and the GO film to block moisture before the start of the test. Two plastic films were used and were aligned without gaps. Initially a GO film was placed on these plastic films with one side held with a weight. One of the plastic films was removed when the test was started; the other plastic film was left in place to hold the GO film at one side with a weight during the test. The GO film bent when it had moisture-assisted actuation ability (Fig. S2†).

## Results and discussion

### Preparation of 1GO and 2GO thin films and characterization of their moisture-induced actuation

The fabrication of the GO thin films and a schematic of their moisture-responsive actuation are shown in Fig. 1. GO thin films were prepared by air-drying an aqueous GO suspension poured into a dish, where the GO self-assembled at the liquid–air interface.<sup>39</sup> After drying, the self-standing GO film was peeled from the dish. Two GO sources with different degrees of oxidation were used in the present study: 1GO and 2GO.<sup>35</sup>

Moisture-responsive actuation was tested at room temperature on a moist substrate heated at 50 °C, where one end was fixed with a weight (Fig. 2). Initially, moisture was blocked by the plastic film, which was subsequently removed to release the moisture; the flipping motion of the 1GO film was then observed (Fig. 2c). Prior to these experiments, we tested a 1GO film fabricated by the commonly used vacuum-assisted filtration method<sup>39,40</sup> and confirmed that both films exhibit highly ordered multilayered structures, as described later (Fig. S1†), and can actuate upon exposure to moisture. We adopted the air-drying method to avoid tedious removal of water from the highly viscous GO suspension and the difficulty associated with peeling the GO film from the filter membrane.

The fabrication procedure of the 2GO films was similar to that of the 1GO films except that a 2GO solution prepared by dissolving the 2GO dry sample in water was used. The moisture-responsive actuation of the 2GO films was also tested, revealing that the 2GO films did not move when exposed to moisture. A distinct difference in the moisture-induced actuation for the 1GO and 2GO films was observed. Because the moisture-induced actuation ability was not lost when a dry sample of 1GO was used (Fig. S2†), we speculated that the loss of the actuation ability of 2GO was not related to the original sample form. To elucidate the origin of the difference in actuation behavior between the 1GO and 2GO films, we compared the particle size distributions in the monolayer GO by AFM (Fig. 3), their oxidation degrees by XPS (Fig. 4 and 5), their multilayered structures by SEM (Fig. 6), their interlayer distances by XRD (Fig. 7), their water absorption (Fig. 8) and diffusion by ATR-FTIR (Fig. 9), and their nanoscale (Fig. 10) and macroscale mechanical properties (Fig. 11).

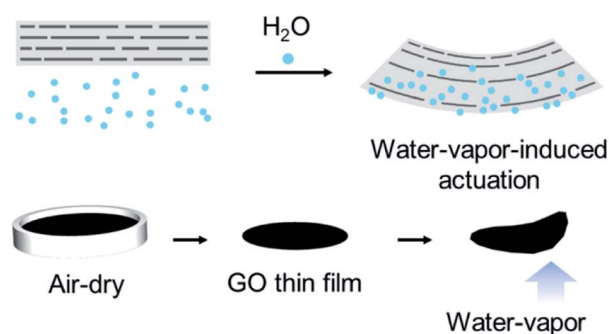


Fig. 1 Schematic of the fabrication process of a GO film and its water-vapor-induced actuation.

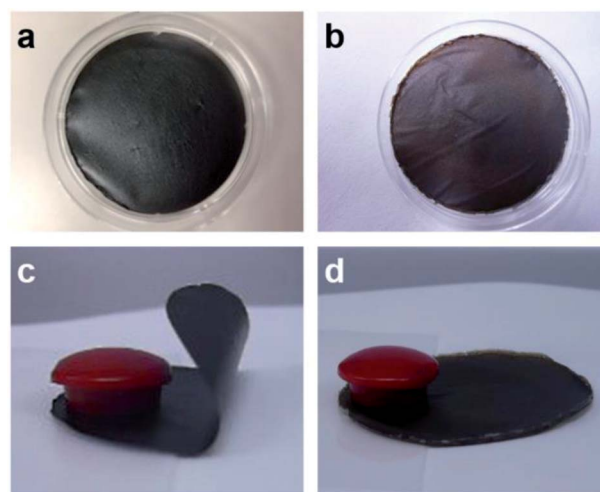


Fig. 2 Photographs of GO thin films prepared by air-drying of an aqueous dispersion of two GO sources: (a) 1GO and (b) 2GO. Different behaviors were observed for the two GO thin films on a moist substrate: (c) actuation of the 1GO film and (d) no actuation of the 2GO film upon exposure to moisture. 1GO: GO prepared by one-cycle oxidation of graphite; 2GO: GO prepared by two-cycle oxidation of graphite. One side of each GO film was fixed on a plastic film. Diameter of the GO films: 50 mm. Thickness of 1GO: 13  $\mu\text{m}$ ; 2GO: 17  $\mu\text{m}$ .

### Size of the GO monolayers

The size of the GO monolayers of 1GO and 2GO before they were incorporated into thin films was investigated by AFM (Fig. 3a

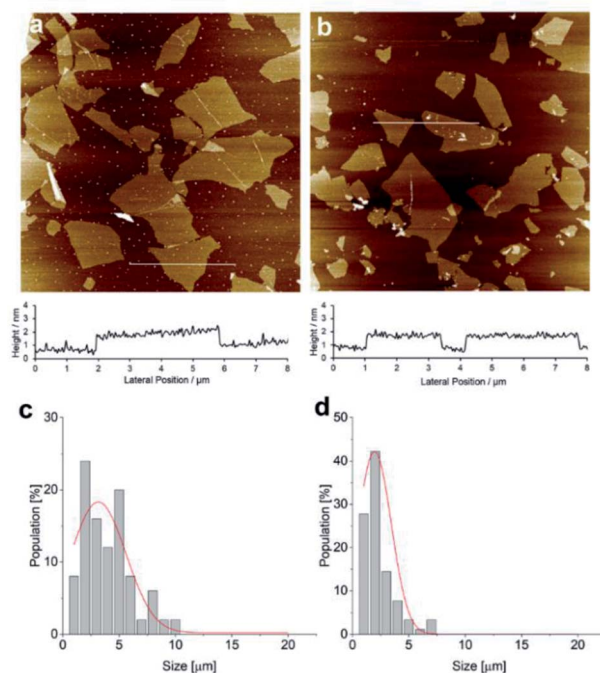


Fig. 3 AFM images and height profiles of (a) 1GO and (b) 2GO films. The histograms ( $N \geq 50$ ) of the size distribution of (c) 1GO and (d) 2GO. Gaussian fits are superimposed as red lines. The long axis of each GO monolayer was measured. Image size: 20  $\mu\text{m}$   $\times$  20  $\mu\text{m}$ .

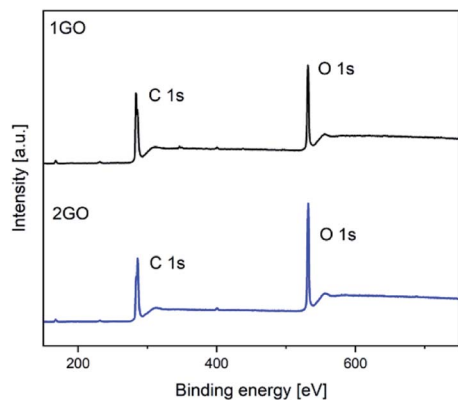


Fig. 4 Survey XPS spectra of 1GO and 2GO films.

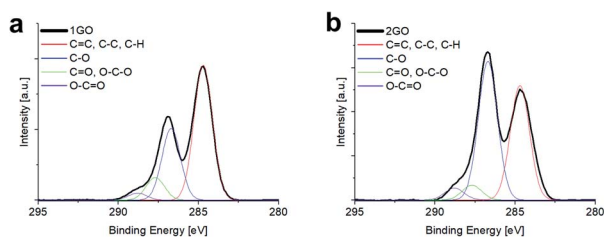


Fig. 5 High-resolution C 1s XPS spectra of (a) 1GO and (b) 2GO films. Curve fitting shows different component peaks with variations in the contents of oxygen-containing functional groups in the GO films. a. u. = arbitrary units.

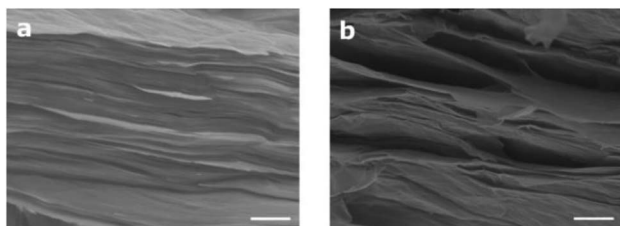


Fig. 6 Cross-sectional SEM images of (a) a 1GO film and (b) a 2GO film, as viewed from a fracture edge. Bars = 1  $\mu\text{m}$ .

and b). The AFM images show that the GO monolayers in both 1GO and 2GO have heights of 1 nm, which is typical for monolayer GO.<sup>33,34,39</sup> The histograms of the size distributions of 1GO and 2GO are shown in Fig. 3c and d. The size distribution histograms of the 1GO and 2GO monolayers are superimposed with the corresponding Gaussian fits of the data, with peaks at  $3.2 \pm 0.4$  and  $2.0 \pm 0.4$   $\mu\text{m}$ , respectively. Thus, 2GO consists of smaller monolayer GO fragments compared with 1GO.

To investigate the effect of monolayer GO size on the moisture-assisted actuation of the films, a 1GO film prepared with fragmented 1GO was tested for moisture-assisted actuation. The fragmented 1GO was obtained by sonication of a 1GO solution for 1 h,<sup>41</sup> and the average size of the GO monolayers was confirmed by AFM to be  $2.1 \pm 0.2$   $\mu\text{m}$  (Fig. S3†). The GO film fabricated using sonicated 1GO demonstrated actuation ability

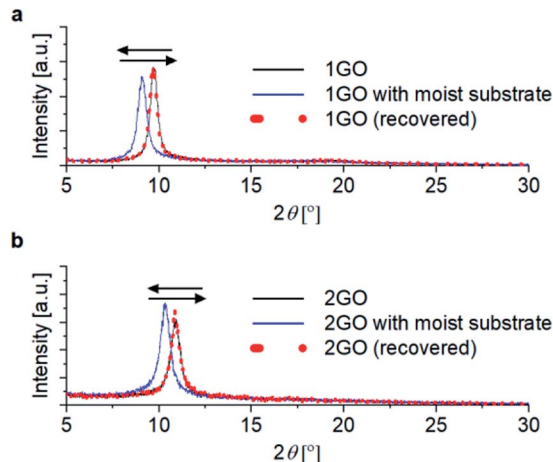


Fig. 7 XRD patterns of (a) 1GO and (b) 2GO thin films (black line), and those with a moist substrate (blue line) and those after removal of the moist substrate (red dots).

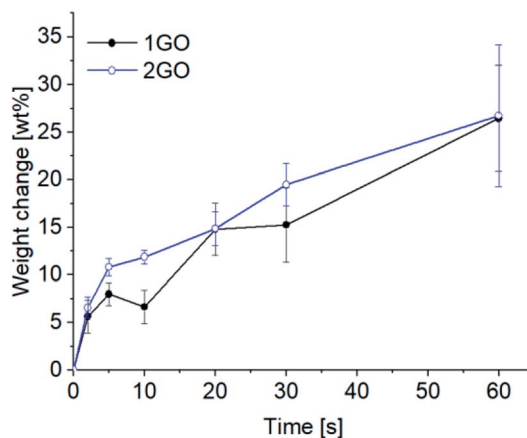


Fig. 8 Time course of the weight change (%) for 1GO (black line) and 2GO (blue line) on a moist substrate because of the adsorption of water ( $N \geq 3$ , error bars = SD).

on a moist substrate. Thus, the level of fragmentation of GO was not the dominant factor responsible for the loss of the moisture-assisted actuation in the 2GO film, although it may affect the moisture-assisted actuation to some extent.<sup>42</sup>

#### Oxidation degree of the GO films

XPS measurements were performed to analyze the difference in chemical composition and bonding between the 1GO and 2GO films. The XPS survey spectra of the 1GO and 2GO films are shown in Fig. 4, and the surface atomic percentages and O/C atomic ratios for the 1GO and 2GO films are listed in Table 1. The O/C atomic ratios for the 1GO and 2GO films were estimated to be 0.37 and 0.48, respectively. The greater oxidation degree of 2GO compared with that of 1GO was confirmed. The main impurity peaks from nitrogen (N 1s) accounted for 1.2% and 1.0% of the 1GO and 2GO thin films, respectively. The



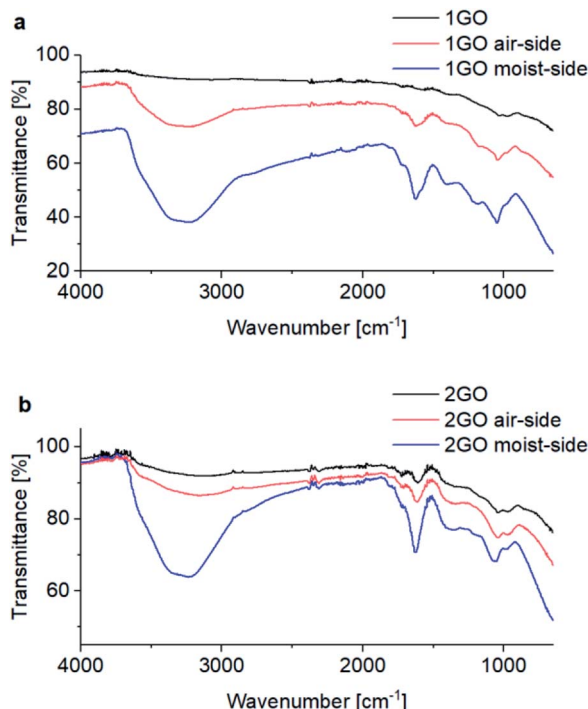


Fig. 9 ATR-FTIR spectra of (a) 1GO and (b) 2GO thin films before (non-treated, black line) and after the moisture-assisted actuation test. The spectra from the bottom side facing the moist substrate (moist side, blue line) and the top side facing the air (air-side, red line) are shown.

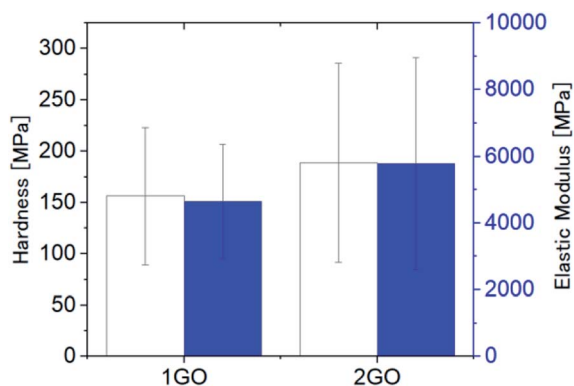


Fig. 10 Hardness (white bars) and elastic modulus (blue bars) of 1GO and 2GO thin films at 50 mN indentation load. ( $N = 20$ , error bar = SD).

content of impurities is essentially unchanged in the 1GO and 2GO films.

High-resolution C 1s XPS spectra for the 1GO and 2GO films are shown in Fig. 5. Each spectrum was fitted into corresponding peaks related to specific bonds (C=C, C-C, C-H (284.7 eV), C-O groups (286.7 eV), C=O, O-C-O (287.7 eV), and O-C=O (288.8 eV)).<sup>43</sup> The contents of each bond type of the 1GO and 2GO films are listed in Table 2. The contents of oxygen-containing functional groups increased in 2GO compared with 1GO.

UV-vis spectra of aqueous dispersions of 1GO and 2GO showed relatively weak absorption intensity of 2GO at visible or

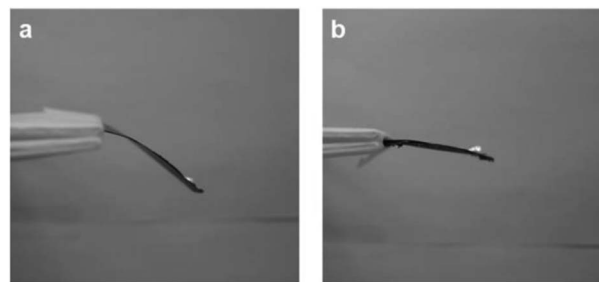


Fig. 11 Distortion of (a) 1GO and (b) 2GO films under an applied weight (20 mg). The length of the GO films from the fulcrum is  $L = 30$  mm.

Table 1 XPS surface atomic percentages and O/C atomic ratios for the 1GO and 2GO films

	1GO	2GO
C 1s	70.9%	66.3%
O 1s	26.3%	32.0%
O/C ratio	0.37	0.48

longer wavelengths, which is consistent with the collapse of the conjugated structure due to the further oxidation degree in 2GO compared with that in 1GO (Fig. S4†).<sup>35</sup>

The energies were calibrated on the basis of the C 1s peak at 284.5 eV. a.u. = arbitrary units.

### Structure of the 1GO and 2GO films

The physical structures of the 1GO and 2GO films were compared. The thickness of the thin films and their moisture-responsive actuation were investigated. The thickness of the thin films was controlled by varying the amount of GO used in the films. The 1GO films with thicknesses of 11 to 22  $\mu\text{m}$  actuated upon moisture contact, whereas the 2GO films with thicknesses of 15 to 19  $\mu\text{m}$  did not. Thus, the thickness in this range was not the dominant factor responsible for the loss of actuation of the 2GO films.

In the cross-sectional SEM images, multilayered structures were observed in both the 1GO and 2GO films (Fig. 6). The thickness of each film, as determined from the SEM images, was 4–5  $\mu\text{m}$  for 1GO and 6–10  $\mu\text{m}$  for 2GO. Measurements with micrometer calipers (1GO: 13  $\mu\text{m}$ ; 2GO: 15  $\mu\text{m}$ ) show that the 2GO film was slightly thicker than the 1GO film. The smaller thickness values obtained from the SEM images compared with those obtained from micrometer caliper measurements

Table 2 XPS peak locations and intensities for 1GO and 2GO films

	1GO	2GO
C=C, C-C, C-H (284.7 eV)	57.1%	40.9%
C-O (286.7 eV)	30.4%	49.5%
C=O, O-C-O (287.7 eV)	9.6%	5.3%
O-C=O (288.8 eV)	2.9%	4.3%

originate from the high-vacuum drying conditions of the samples prepared for SEM observation.

The interlayer spacings of the GO thin films with and without the moist substrate were investigated by XRD analysis. The representative spectra are shown in Fig. 7. Since the difference in the moisture actuation ability of 1GO and 2GO was retained from the day the samples were freshly prepared to after more than 10 months, XRD analysis was performed with substrates that have various aging times and the average values with standard deviations are shown. The peaks for 1GO and 2GO without the moist substrate showed interlayer distances of  $8.44 \pm 0.41$  Å and  $8.31 \pm 0.17$  Å, with no significant difference between the 1GO and 2GO thin films. The interlayer distances increase with the moist substrate to  $9.04 \pm 0.46$  Å and  $8.73 \pm 0.18$  Å for 1GO and 2GO, respectively. When the moist substrate was removed, the distance was precisely returned to the original state for both 1GO and 2GO. The interlayer distances in water were 10.2 Å and 12.4 Å for 1GO and 2GO, respectively (Fig. S5†).

### Adsorption of moisture

The time course of the amount of adsorbed moisture was examined for the 1GO and 2GO thin films from 2 to 60 s (Fig. 8). Contrary to the expectation from the results of the actuation experiments, no substantial difference was observed between the 1GO and 2GO films. Given that moisture-assisted actuation starts within 1 s and lasts for more than 1 min, the affinity to water is the same in the films. Thus, water affinity cannot be the major factor responsible for the different actuation behaviors between the 1GO and 2GO films.

The interlayer-diffusion of water in the 1GO and 2GO thin films was analyzed by measuring ATR-FTIR at both the moist and air sides of the films before and after the moisture-assisted actuation test (Fig. 9).<sup>44</sup> Both the 1GO and 2GO thin films showed representative peaks of  $\nu(\text{OH})$  at  $3240\text{ cm}^{-1}$  and  $1620\text{ cm}^{-1}$ ,  $\nu(\text{C}=\text{O})$  at  $1620\text{ cm}^{-1}$ , and  $\nu(\text{epoxide})$  at  $1050\text{ cm}^{-1}$ . Although the intensities of the peaks of  $\nu(\text{OH})$  at  $3240\text{ cm}^{-1}$  were increased at the moist (bottom) side of the GO films, those of the air (top) side are moderate. The results indicate that the asymmetric content of water at the bottom and top side of the films is maintained both in 1GO and 2GO in the moisture assisted actuation test, which is necessary for actuation.

### Mechanical properties of the GO films

The mechanical properties of the GO films were characterized using nanoindentation measurements. The nanoindentation experiments were carried out using a nanoindenter in conjunction with the method of CSM. The hardness of the 1GO and 2GO films was  $156 \pm 67$  MPa and  $189 \pm 97$  MPa, and the elastic modulus of the films was  $4.7 \pm 1.7$  GPa and  $5.8 \pm 3.2$  GPa, respectively (Fig. 10). Both the hardness and elastic modulus values are consistent with those previously reported for GO films.<sup>45</sup> Although the average hardness and elastic modulus values for the 2GO films are greater than those of the 1GO films, a statistical difference between the two samples was not detected because of the nonuniformity of the samples at the nanoscale.

To evaluate the macroscopic mechanical properties of the GO films, we examined the degree of bending of the films under an applied weight. One side of the films was fixed, and a weight was placed on the other side to measure the strain of the films. When the applied weight (20 mg) was approximately the same as that of the 1GO and 2GO films, the 1GO film bent ( $\epsilon = 0.025 \pm 0.006\%$ ), whereas the 2GO film only slightly bent ( $\epsilon = 0.012 \pm 0.004\%$ ) (Fig. 11). The experiments were conducted on the same day so that the effect of differences in humidity<sup>46</sup> would be negligible. Similar results were observed when the applied weight was 2.5 times the weight of the films (50 mg,  $\epsilon = 0.015\%$ , ESI Table S1†). Thus, the 2GO film was confirmed to be more difficult to bend in the out-of-plane direction than the 1GO film. Given that the GO films exert a maximum force sufficient to lift a weight approximately equal to their own weight upon adsorbing water,<sup>42</sup> the distinct difference between the moisture-assisted actuation behaviors of the 1GO and 2GO films might originate from the difference in hardness between the films.

Enhanced interlayer interactions *via* hydrogen bonding through additional molecules have been reported to enhance the mechanical properties of GO films.<sup>47–49</sup> Increased oxygen-containing functional groups in 2GO can enhance the interlayer interactions and mechanical strength. For multilayer films, their mechanical properties are determined by both the properties of the single layer and the interlayer interactions. Thus, although the flexibility of a single layer of more extensively oxidized 2GO may increase as a result of the structural change from  $\text{sp}^2$  carbon to  $\text{sp}^3$  carbon, the increased hydrogen bonding due to further oxidation may hamper the flexible motion of the monolayers. As a result, bending of the more oxidized 2GO films is considered to become more difficult than that of the 1GO films.

## Conclusions

The material obtained by chemical oxidation of graphite and dispersed into a single layer is categorized as GO. The size, shape, degree of oxidation, and type and/or amount of chemical functionalities of GO differ greatly depending on the method used to prepare it. The mechanical, physical, and chemical properties of GO therefore also differ substantially depending on the preparation method. Although GO has been reported to have attractive functionality for biological applications, conductive materials, and actuation materials, the relationship between functionality and the degree of oxidation of GO films has not been fully elucidated.

In the present study, we found that moisture-induced actuation in GO multilayered films (1GO) is lost in GO multilayered films prepared from GO with a higher oxidation degree as a result of two-cycle oxidation (2GO), where the oxidation degrees were confirmed by XPS analysis. For most of the characteristic properties, no distinct difference was observed between the 1GO and 2GO films: AFM imaging revealed that 2GO consists of slightly smaller fragments of monolayers compared to 1GO, although this difference did not substantially affect vapor-induced actuation, and SEM observations revealed that both films consisted of multilayered structures with no

substantial differences in the interlayer distances from XRD measurements. Both films adsorbed moisture at a similar rate on timescales from seconds to 1 min while retaining a different water content at the bottom and top side. Nanoindentation experiments indicated that both films showed hardness and elasticity typical of GO films, with no substantial difference between the 1GO and 2GO films. However, a clear difference was observed in the macroscopic mechanical properties: the 1GO film bent under a weight similar to that of the thin film, whereas the 2GO film hardly bent under the same conditions. Given that GO films can lift their own weight (at most), such a difference in mechanical characteristics is likely a decisive factor in the difference between the moisture actuation behaviors of the two films. Our finding—that the oxidation degree of GO dramatically affects its moisture-induced actuation—emphasizes the importance of controlling the chemical structure of functional materials, as is the case in organic materials. Precise control of the functional groups and carbon structure of GO will further expand the development and scope of GO-based materials.

## Author contributions

W. N. conceived, directed and performed the experiments. Y. Y. performed the nanoindentation experiments. M. Y. directed the XRD experiments. Y. N. provided GO samples. All authors discussed and wrote the manuscript.

## Conflicts of interest

There are no conflicts to declare.

## Acknowledgements

We acknowledge Ms. Naoko Sato for assistance with experiments. Part of this work was supported by the Materials Analysis Station, NIMS. We acknowledge Mr Hirohito Ohata (NIMS) for XPS measurements and Dr Toshikazu Iwata (TOYO Corporation) for the nanoindentation measurements. This work was partially supported by JSPS KAKENHI Grant Numbers, 18H05419 (Molecular Engine) and 20H05224 (Aquatic Functional Materials).

## Notes and references

- 1 Z.-C. Jiang, Y.-Y. Xiao, X. Tong and Y. Zhao, *Angew. Chem., Int. Ed.*, 2019, **58**, 5332–5337.
- 2 W.-C. Xu, S. Sun and S. Wu, *Angew. Chem., Int. Ed.*, 2019, **58**, 9712–9740.
- 3 F. Ge and Y. Zhao, *Adv. Funct. Mater.*, 2019, **30**, 1901890.
- 4 D. Dattler, G. Fuks, J. Heiser, E. Moulin, A. Perrot, X. Yao and N. Giuseppone, *Chem. Rev.*, 2020, **120**, 310–433.
- 5 F. Amir, X. Li, M. C. Gruschka, N. D. Colley, L. Li, R. Li, H. R. Linder, S. A. Sell and J. C. Barnes, *Chem. Sci.*, 2020, **11**, 10910–11920.
- 6 S. B. Abel, C. R. Rivarola, C. A. Barbero and M. Molina, *RSC Adv.*, 2020, **10**, 9155–9164.
- 7 T. Gao, G. Xu, Y. Wen, H. Cheng, C. Li and L. Qu, *Nanoscale Horiz.*, 2020, **5**, 1226–1232.
- 8 J. Li, X. Li, Z. Zheng and X. Ding, *RSC Adv.*, 2019, **9**, 13168–13172.
- 9 B. Wu, Y. Jian, X. Le, H. Lin, S. Wei, W. Lu, J. Zhang, A. Zhang, C.-F. Huang and T. Chen, *ACS Appl. Mater. Interfaces*, 2019, **11**, 48564–48573.
- 10 C. Li, H. Xia and Q.-Q. Ni, *Langmuir*, 2020, **36**, 14933–14941.
- 11 M. R. O'Neill, E. Acome, S. Bakarich, S. K. Mitchell, J. Timko, C. Keplinger and R. F. Shepherd, *Adv. Funct. Mater.*, 2020, **30**, 2005244.
- 12 Y. Song, S. Qin, J. Gerringer and C. Grunlan, *Soft Matter*, 2019, **15**, 2311–2314.
- 13 Z. Zheng, H. Wang, L. Dong, Q. Shi, J. Li, T. Sun, Q. Huang and T. Fukuda, *Nat. Commun.*, 2021, **12**, 411.
- 14 Y. Park and X. Chen, *J. Mater. Chem. A*, 2020, **8**, 15227–15244.
- 15 K. Sano, Y. Ishida and T. Aida, *Angew. Chem., Int. Ed.*, 2018, **57**, 2532–2543.
- 16 M. Ma, L. Guo, D. G. Anderson and R. Langer, *Science*, 2013, **339**, 186–189.
- 17 C. Li, A. Iscen, H. Sai, K. Sato, N. A. Sather, S. M. Chin, Z. Álvarez, L. C. Palmer, G. C. Schatz and S. I. Stupp, *Nat. Mater.*, 2020, **19**, 900–909.
- 18 X. Chen, D. Goodnight, Z. Gao, A. H. Cavusoglu, N. Sabharwal, M. DeLay, A. Driks and O. Sahin, *Nat. Commun.*, 2015, **6**, 7346.
- 19 W. Nakanishi, K. Minami, L. K. Shrestha, J. Qingmin, J. P. Hill and K. Ariga, *Nano Today*, 2014, **9**, 378–394.
- 20 K.-L. Zhang, Z.-L. Hou, B.-X. Zhang and Q.-L. Zhao, *Appl. Phys. Lett.*, 2017, **111**, 153101.
- 21 B.-H. Wee, W.-H. Khoh, A. K. Sarker, C.-H. Lee and J.-D. Hong, *Nanoscale*, 2015, **7**, 17805–17811.
- 22 H. Bi, K. Yin, X. Xie, J. Ji, S. Wan, L. Sun, M. Terrones and M. S. Dresselhaus, *Sci. Rep.*, 2013, **3**, 2714.
- 23 Z. Zhang, W. Shen, L. Lin, M. Wang, N. Li, Z. Zheng, F. Liu and L. Cao, *Adv. Sci.*, 2020, **7**, 2000286.
- 24 F. Zhao, H. Cheng, Z. Zhang, L. Jiang and L. Qu, *Adv. Mater.*, 2015, **27**, 4351–4357.
- 25 Y. Liang, F. Zhao, Z. Cheng, Y. Deng, Y. Xiao, H. Cheng, P. Zhang, Y. Huang, H. Shao and L. Qu, *Energy Environ. Sci.*, 2018, **11**, 1730–1735.
- 26 W. Xuan, M. He, N. Meng, X. He, W. Wang, J. Chen, T. Shi, T. Hasan, Z. Xu, Y. Xu and J. K. Luo, *Sci. Rep.*, 2014, **4**, 7206.
- 27 T.-Y. Zhang, Q. Wang, N.-Q. Deng, H.-M. Zhao, D.-Y. Wang, Z. Yang, Y. Liu, Y. Yang and T.-L. Ren, *Appl. Phys. Lett.*, 2017, **111**, 121901.
- 28 G. Nam and J.-Y. Leem, *RSC Adv.*, 2015, **5**, 94222–94226.
- 29 H. Chi, Y. J. Liu, F. Wang and C. He, *ACS Appl. Mater. Interfaces*, 2015, **7**, 19882–19886.
- 30 A. Iakunkov and A. V. Talyzin, *Nanoscale*, 2020, **12**, 21060–21093.
- 31 P. P. Brisebois and M. Sijaj, *J. Mater. Chem. C*, 2020, **8**, 1517–1547.
- 32 A. T. Smith, A. M. LaChance, S. Zeng, B. Liu and L. Sun, *Nano Mater. Sci.*, 2019, **1**, 31–47.
- 33 A. T. Dideikin and A. Y. Vul', *Front. Phys.*, 2019, **6**, 149.
- 34 S. Ye and J. Feng, *RSC Adv.*, 2016, **6**, 39681–39687.

- 35 N. Morimoto, T. Kubo and Y. Nishina, *Sci. Rep.*, 2016, **6**, 21715.
- 36 X. Li and B. Bhushan, *Mater. Charact.*, 2002, **48**, 11–36.
- 37 W. C. Oliver and G. M. Pharr, *J. Mater. Res.*, 1992, **7**, 1564–1583.
- 38 I. Takeuchi, K. Asaka, K. Kiyohara, T. Sugino, N. Terasawa, K. Mukai, T. Fukushima and T. Aida, *Electrochim. Acta*, 2009, **54**, 1762–1768.
- 39 C. Chen, Q.-H. Yang, Y. Yang, W. Lv, Y. Wen, P.-X. Hou, M. Wang and H.-M. Cheng, *Adv. Mater.*, 2009, **21**, 3007–3011.
- 40 V. Kohlschütter and P. Haenni, *Z. Anorg. Allg. Chem.*, 1919, **105**, 121–144.
- 41 S. Yea and J. Feng, *RSC Adv.*, 2016, **6**, 39681–39687.
- 42 Y. Ge, R. Cao, S. Ye, Z. Chen, Z. Zhu, Y. Tu, D. Ge and X. Yang, *Chem. Commun.*, 2018, **54**, 3126–3129.
- 43 T. R. Gengenbach, G. H. Major, M. R. Linford and C. D. Easton, *J. Vac. Sci. Technol., A*, 2021, **39**, 013204.
- 44 W. Guo, J. Chen, S. Sun and Q. Zhou, *J. Phys. Chem. C*, 2016, **120**, 7451.
- 45 A. Knöller, C. P. Lampa, F. von Cube, T. H. Zeng, D. C. Bell, M. S. Dresselhaus, Z. Burghard and J. Bill, *Sci. Rep.*, 2017, **7**, 40999.
- 46 A. V. Talyzin, G. Mercier, A. Klechikov, M. Hedenström, D. Johnels, D. Wei, D. Cotton, A. Opitz and E. Moons, *Carbon*, 2017, **115**, 430–440.
- 47 R. Jalili, S. H. Aboutalebi, D. Esrafilzadeh, E. L. Shepherd, J. Chen, S. Aminorroaya-Yamini, K. Konstantinov, A. I. Minett, J. M. Razal and G. G. Wallace, *Adv. Funct. Mater.*, 2013, **23**, 5345–5354.
- 48 O. C. Compton, S. W. Cranford, K. W. Putz, Z. An, L. C. Brinson, M. J. Buehler and S. T. Nguyen, *ACS Nano*, 2012, **6**, 2008–2019.
- 49 N. V. Medhekar, A. Ramasubramaniam, R. S. Ruoff and V. B. Shenoy, *ACS Nano*, 2010, **4**, 2300–2306.